scientific reports

Check for updates

OPEN

# Achieving bifacial photovoltaic performance in PTB7-based organic solar cell by integrating transparent contact for emerging semi-transparent applications

Erman Çokduygulular[1]✉, Çağlar Çetinkaya[2], Serkan Emik[3] & Barış Kınacı[4,5]

**In this study, the design, fabrication and detailed analysis of semi-transparent bifacial organic solar cells (ST-OSC) based on $MoO_3$/Ag/$WO_3$ (10/$d_m$/$d_{od}$ nm) dielectric/metal/dielectric (DMD) transparent contact system integrated with PTB7 polymer were investigated. The study emphasizes the importance of designing transparent contact systems to optimize the solar cells' transparency (average visible transmittance, AVT), color rendering (color rendering index, CRI), efficiency (power conversion efficiency, PCE), and bifaciality. The performance of three distinct configurations was examined in the $AVT_{max}$ (47.14% AVT, 3.93% PCE), $(CRI_{ext})_{max}$ (23.82% AVT, 6.21% PCE), and Extreme Color (26.34% AVT, 5.81% PCE). The theoretically predicted AVTs for these configurations were 48.75%, 22.29%, and 25.15%, respectively. The strong agreement between theoretical and observed outcomes confirmed the accuracy of the Transfer Matrix Model (TMM). Furthermore, the assessment of bifaciality performance exhibited that the $AVT_{max}$ had a bifaciality factor of 0.94, with a PCE of 3.67% under top illumination and 3.93% under bottom illumination. The high bifaciality of the structure designed with TMM to maximize the AVT demonstrates the value of calculations prior to solar cell structure fabricating and the possibility of constructing high bifaciality structures using this technique.**

**Keywords** Semi-transparent organic solar cells, Light management engineering, PTB7:$PC_{71}BM$, Color rendering index, $MoO_3$/Ag/$WO_3$ transparent contact, Bifaciality

Organic solar cells (OSCs), which enable the expansion of the application areas of photovoltaic technology, have gained significant prominence in science and industry due to their numerous advantages[1,2]. Furthermore, cutting-edge solutions for urban architecture have been made possible by the development of semi-transparent (ST) solar cells, which seamlessly integrate solar energy harvesting capabilities into facades and windows without sacrificing aesthetics. By integrating these cells into windows, facades, and other transparent surfaces, buildings can utilize solar energy without sacrificing natural light or obstructing the view[3]. Particularly, when considering building-integrated photovoltaics (BIPV), creating energy-efficient structures serving both functional and aesthetic purposes will be achievable. This situation signifies a movement towards the seamless integration of renewable energy solutions into our daily lives and further emphasizes the importance of solar energy in shaping a sustainable future[3,4].

OSCs promise to provide energy to support the Internet of Things (IoT) ecosystem, including remote sensors, calculators, smart meters, wearables and communication devices, which are increasingly being adopted in various applications such as smart homes, factories, offices and wearable technology. IoT, in particular, has significant potential to improve life quality. In advanced next-generation IoT ecosystems, powering many IoT devices with batteries will be unsustainable from an environmental, resource, security and cost perspective. Therefore, with the use of indoor photovoltaics (IPVs), it will be possible to ensure stable power generation by

[1]Department of Engineering Sciences, Faculty of Engineering, Istanbul University-Cerrahpaşa, Istanbul TR-34320, Türkiye, Turkey. [2]Physics Department, Faculty of Science, Istanbul University, Istanbul TR-34134, Türkiye, Turkey. [3]Department of Chemical Engineering, Faculty of Engineering, Istanbul University-Cerrahpaşa, Istanbul TR-34320, Türkiye, Turkey. [4]Department of Photonics, Faculty of Applied Sciences, Gazi University, Ankara TR-06500, Türkiye, Turkey. [5]Photonics Application and Research Center, Gazi University, Ankara TR-06500, Türkiye, Turkey. ✉email: erman.cokduygulular@iuc.edu.tr

using energy from the illuminated environment[5,6]. In addition, owing to the significant absorption of the visible spectrum, ST-OSC devices have the potential for use under indoor illumination[7]. The inherent versatility of OSC technology enhances appeal by allowing creative integration into various surfaces, such as small electronic devices, windows, walls and even textiles[7].

Semi-transparent organic solar cells represent a significant advance in photovoltaic technology by taking advantage of the unique properties of polymers to increase flexibility, transparency and efficiency in solar energy conversion. The planned structures of semi-transparent solar cells and energy production can reduce energy consumption due to their transparency[8,9]. The solution-based method for processing organic compounds has reduced production-related challenges and significantly lowered costs. Therefore, with their potential for low-cost and environmentally friendly processes, organic solar cells have emerged as candidates for next-generation solar cell technology compared to traditional inorganic solar cells, enabling the production of large-area, ultra-thin, lightweight, flexible, and low-cost devices[1]. Companies seeking to commercialize OSCs aim to target device applications for the outdoor market, such as flexible and mobile modules or semi-transparent solar cells for windows, thereby aiming for building integration[10–12].

The design of transparent contacts with enhanced optical properties to reduce reflection and absorption in visible light without altering the energy band structure and providing selective transport in the solar cell structure is crucial for high-performance semi-transparent organic solar cells[8,13]. Generally, thick metal electrodes such as Ag, Au, and Al are used in organic solar cells. However, when these metals are thick, they become highly opaque and reflect in the visible region[8]. In the pursuit of transparency in semi-transparent organic solar cells, the use of dielectric/metal/dielectric (DMD) transparent contact designs can be considered. These designs offer high optical transparency and electrical conductivity, low haze, exceptional flexibility, ease of fabrication and compatibility with various substrates[8,14–17]. The DMD design sandwiches a thin metal material between two anti-reflection dielectrics, and the optical properties can be varied by the thickness of these layers. It is possible to design DMD transparent electrodes with low reflectance properties, thereby allowing careful adjustment of photon absorption in the device to enable sufficient light transmission through the device[17,18].

In semi-transparent optoelectronic devices, there is typically a balance between light transmission and absorption; hence, the consideration of optical optimization is crucial in the design of ST-OSCs. Furthermore, optical modifications in ST-OSCs can affect the material's electrical performance while altering the organic material's optical characteristics, constituting the active region. This can lead to adverse effects on photovoltaic performance. Therefore, modifying the propagation of electromagnetic waves within the ST device without disrupting the active organic material is a highly functional approach[8,14–17]. Light management engineering-based approaches have been employed to optimize the optical properties of ST-OSCs[19–21]. Among these approaches, using the Transfer Matrix Method (TMM) is a highly effective approach for improving and modifying optical characteristics[8,14,15,22,23].

In addition, the fact that the active regions of organic semiconductor-based solar cells are in a bulk-heterojunction configuration allows photo-generated carriers to be efficiently swept to the contacts by the internal electric field, regardless of whether the light enters the active region from the n or p side, unlike in inorganic semiconductors. This characteristic enables the production of high-performance bifacial solar cells that can operate independently of which side the light enters the active region, thus utilizing solar energy efficiently. Unlike conventional monofacial solar cells, bifacial solar cells can harness direct sunlight and reflected light from the ground, surrounding objects, or artificial light sources. This dual-sided energy generation capability results in higher efficiency and energy output. However, bifacial solar cells differ from monofacial solar cells in that they have several design prerequisites. The most crucial of these is integrating a transparent top contact and hole transport layer (HTL) layers into the cell to ensure that light entering from the back surface can effectively reach the active region. Thus, bifacial solar cells should provide a symmetrical optical path within the cell for electromagnetic waves to propagate. For this reason, it is vital to develop transparent contacts with a bandgap larger than that of the active region, as well as to align the band edges of other cell materials to provide an appropriate band alignment. In OSCs, efficient bifacial architectures can be designed with anti-reflective coatings and photonic-based DMD transparent top contact structures as an alternative to ITO, allowing light to enter the cell more effectively. Therefore, high transparency in electron transport layer (ETL), HTL, and contact systems makes these OSCs efficient optoelectronic devices capable of bifacial operation. These innovative photonic-based bifacial cell designs focus on optimizing the active regions and the selective transmission layers, electrodes, and integrated photonic structures. DMD transparent electrodes play a critical role in adjusting the electrical and optical properties of semi-transparent optoelectronic devices and bifacial solar cells[17].

In 2010, Liang and Yu[24] proposed a series of medium bandgap polymers called the PTB series, with bandgaps ranging from 1.7 to 1.84 eV. These series exhibited efficient absorption in the solar spectrum in the highest intensity photon flux region (400–700 nm range). PTB series polymers have the potential to form structures with high hall mobility thanks to their rigid backbone. The appropriate side chains in the polymer backbone not only dissolve well with fullerene acceptors but also form favorable blends. The structural flexibility in the polymer backbone results in relatively low highest occupied molecular orbital (HOMO) energy levels compared to polymers, leading to improvements in photovoltaic parameters. Hence, an increase in Power Conversion Efficiency (PCE) is observed. Additionally, it can be stated that the polymer series are efficient materials for solar energy conversion and can potentially achieve higher efficiencies through research and development efforts[24]. The PCEs for structures sequentially proposed from PTB1 to PTB6 vary between 2.26% and 5.53% [24]. In a different study conducted by the same research group, the PTB7 polymer with an extended absorption edge to 750 nm, achieved the highest efficiency of the PTB series with a value of 7.5% [25]. These studies indicate a promising future for structures containing PTB series polymers in organic solar cell researches[24,25].

Upon examination of studies on PTB7, it has been observed that the blend formed with the $PC_{71}BM$ polymer exhibits high transparency in the visible region[1,19,26–28]. In a study where the active region consisted of the

PTB7:$PC_{71}BM$ blend, Liu et al. achieved a PCE of 3.4% for a structure with a 40% average visible transmittance (AVT)[26]. In another study, Fan et al. obtained a PCE of 3.75% for a structure with a 35% AVT[27]. However, it has been observed that it is possible to waive one of the AVT or PCE values and increase the other with different structure designs. Xu et al. obtained a PCE of 5.9% in a structure with an AVT of 22% [19]. In another study, Zheng et al. found the PCE to be 3% for a structure with an AVT of 47.5% [28].

In recent years, research has focused on the development of novel donor and acceptor molecules to reduce energy loss in the active layer and improve the efficiency of OSCs. Notably, PCEs of up to 19% have been achieved with non-fullerene acceptors (NFAs), thanks to their adaptable chemical structures and finely tuned band gaps, energy levels, and crystallization. The arrangement of these NFAs is crucial for optimizing light absorption, phase separation, and charge transport in photovoltaic mixtures, which directly impacts the PCE. For example, Donghui Li and colleagues increased the PCE from 16 to 19% by refining the fibril structure of the NFA L8-BO with the solvent additive 1-fluoronaphthalene (FN). Similarly, Gao et al. surpassed 19% efficiency in planar mixed heterojunction OSCs by introducing asymmetric selenium substitution in the electron acceptor BS3TSe-4 F. Additionally, adopting green solvents like ortho-xylene (o-XY) to fabricate OSCs offers a more environmentally friendly alternative to hazardous solvents such as chlorobenzene, improving efficiency and sustainability[13].

In the context of the study, the optimal structures determined in our previous study[13] were fabricated by integrating the asymmetric $MoO_3/Ag/WO_3$ DMD transparent contact system to OSCs with the active region consisting of a novel polymer PTB7:$PC_{71}BM$ bulk-heterojunction (BHJ) blend. Following the fabrication of the structures with different optimal features, their optical characteristics and photovoltaic parameters, such as AVT, PCE, and bifaciality were experimentally determined, and theoretical and experimental comparisons were made. This research explores the trade-offs between transparency and efficiency by comparing different structural configurations, providing insights into optimizing OSCs for practical applications. The fabricated ST-OSCs achieved an AVT of 47.14% and PCE of 3.93%, closely aligning with theoretical calculations (48.75% for maximum AVT) made using the TMM. In addition, the bifacial properties of the fabricated organic solar cells were compared both theoretically and experimentally, revealing a bifaciality factor of 0.94 for the maximum AVT structure, with a top illumination PCE of 3.67% compared to 3.93% under bottom illumination. The study's findings contribute to the growing body of knowledge in organic photovoltaics, highlighting the importance of material, layer thickness control, and structural design in achieving semi-transparent organic solar cells.

## Result and discussion

Within the scope of the study, a highly fine-tuned $MoO_3/Ag/WO_3$ ($10/d_m/d_{od}$ nm) DMD transparent top contact system was integrated into a PTB7-based organic solar cell to fabricate transparent solar cells having high bifaciality with outstanding optical performance designed in a suitable structure architecture and their experimental photovoltaic performances were analyzed. Considering the application potential of integrated ST-OSCs, it is imperative to design DMD transparent contact systems that can be finely tuned. In order to use ST-OSCs in window applications, it is desirable for the DMD system to offer optical properties at high AVT and near to D65 point or the Planckian locus or various color coordinates[14,29]. Having a neutral color and a high color rendering index (CRI) are other design parameters that ST-OSCs should aim for[8,14]. The exceptional optical properties exhibited are directly linked to the wavelength-dependent characteristics of the refractive indices (n) and extinction coefficients ($k_{ex}$) of all structures comprising the ST-OSC. These are directly related to the thickness of the top and bottom dielectric materials and the very thin metallic layer in the integrated DMD system. That is why, for the semi-transparent PTB7-based OSC with outstanding optical performance investigated in this study, as theoretically investigated in our previous work[13], AVT, CRI, and color properties of the integrated asymmetric $MoO_3/Ag/WO_3$ DMD transparent top contact system are evaluated in detail using the Transfer Matrix Method (TMM). In this study, the fabrication of these optimal structures and their experimental photovoltaic performances have been evaluated, and their bifacial properties have been examined. The study especially examines the bifacial working conditions of $AVT_{max}$, $(CRI_{ext})_{max}$ and Extreme Color architectures, which we previously only studied theoretically and determined optimally. Before that, an experimental evaluation of the optical and photovoltaic parameters previously presented theoretically is presented comparatively.

In the investigated OSCs, fluorine-doped tin oxide (FTO), which has high optical transmittance and electrical conductivity and low work function (4.4 eV), was employed as the transparent sub-contact system[30]. Regardless of fluorine doping, FTO offers outstanding optical transparency (> 90%) throughout the visible range[30,31]. In addition, FTO can be fabricated at a lower cost compared to indium-doped tin oxide (ITO), commonly used in conventional structures, and its dependence on the cleaning procedure for the work function is lower[30]. In inverted OSCs, zinc oxide (ZnO), characterized by its n-type metal-oxide properties and notable carrier mobility, is employed as the hole-blocking layer. ZnO has a conduction band energy of approximately − 4.4 eV and a valence band energy of -7.4 eV. This band feature facilitates the transport of electrons generated within the active region to ZnO, concurrently impeding the transition of holes[30]. Due to this role, ZnO is also referred to as the ETL in OSCs. Additionally, due to its wide bandgap, ZnO offers high optical transparency in the visible and near-infrared (NIR) regions, allowing photons to reach the active region efficiently[8,32,33]. A 30 nm thickness ZnO ETL is suitable for effective electron transport, optical transmission and hole blocking[34]. Considering these reasons, the ZnO thickness was chosen as 30 nm in the designed OSCs.

Poly ({4,8-bis[(2-ethylhexyl)oxy]benzo[1,2-b: 4,5-b0]dithiophene- 2,6-diyl}{3-fluoro-2-[(2-ethylhexyl) carbonyl]thieno[3,4-b]thiophenediyl}) (PTB7) served as the donor polymer, while (6,6)-phenyl $C_{71}$ butyric acid methyl ester ($PC_{71}BM$), a fullerene derivative distinguished by its high electronegativity and excellent charge transport properties, was utilized as the acceptor polymer[35]. The PTB7:$PC_{71}BM$ blend in BHJ configuration represents an innovative absorber system characterized by a 3.7 eV electron affinity, 0.9 eV band gap, and notable carrier mobility. Due to these features, it is frequently used in ST-OSC structures with superior optical and

photovoltaic performance[22,36–38]. In the design of ST-OSCs, the thickness optimization of the BHJ PTB7:$PC_{71}BM$ blend forming the active region is crucial, considering parameters such as excellent absorption characteristics, mechanical durability, environmental stability, efficient exciton generation and separation, and most importantly, good transparency in the visible range. Almost all of these parameters are thickness-dependent and in trade with each other[39]. Therefore, numerous studies have been conducted in the literature on optimizing the thickness of the BHJ PTB7:$PC_{71}BM$ blend[39]. Based on photovoltaic performance parameters such as fill factor (FF), short-circuit current density ($J_{sc}$), open-circuit voltage ($V_{oc}$), PCE, and essential optical values such as AVT, it has been observed that the BHJ PTB7:$PC_{71}BM$ blend at a thickness of 100 nm exhibits optimal performance for ST-OSCs[36,39]. Therefore, the absorber layers of ST-OSCs with BHJ PTB7:$PC_{71}BM$ blend were designed with a thickness of 100 nm.

Molybdenum trioxide ($MoO_3$) has been employed as both the HTL and the inner dielectric layer in the ST-OSCs. In opaque OSCs featuring a thick metal layer, the $MoO_3$ layer functions solely as a HTL. However, in ST-OSCs, it serves a dual role as both an HTL and the inner dielectric component of the transparent top contact within the DMD structure. In addition, the $MoO_3$ HTL layer prevents metal penetration into the active region in all OSCs. $MoO_3$ exhibits high hole mobility and high transparency in the visible range[8,32]. With a conduction band energy of approximately − 2.3 eV and a valence band energy of -5.3 eV, $MoO_3$ exhibits properties conducive to efficient hole transport. Therefore, holes generated within the active region and subsequently separated can be effectively conveyed to $MoO_3$ while electrons are blocked from further movement[30]. For this reason, numerous studies have been conducted on the design of high-performance optoelectronic devices utilizing $MoO_3$ as the HTL among the TCOs with high work function[15,40].

A comparison of a conventionally designed opaque organic solar cell and a semi-transparent organic solar cell designed for optimal optical properties is shown in Fig. 1. For ST-OSCs, the Transition metal oxide (TMO) based transparent top contact structure is designed in an asymmetric $MoO_3$/Ag/$WO_3$ DMD configuration. Transparent contact designs containing $MoO_3$ and $WO_3$ are commonly used in displays, tunable mirrors, and energy-efficient smart windows. Such systems have exhibited extremely encouraging performances in electrochromic devices, where transparency, color or other optical features can be adjusted in response to the applied potential[15,29,41]. That is why, among various TMOs, DMD systems with $MoO_3$ and $WO_3$ have been extensively studied in the literature[29,42]. Moreover, for inverted ST-OSCs, asymmetric $MoO_3$/Ag/$WO_3$ transparent contact systems are more effective than symmetric DMD systems of $MoO_3$/Ag/$MoO_3$ and $WO_3$/Ag/$WO_3$. As previously mentioned, $MoO_3$ as the inner dielectric layer exhibits a favorable HTL performance, while $WO_3$ as the outer dielectric is of particular interest among electrochromic materials due to its high coloring efficiency, chemical stability and strong adhesion to various substrates[15,43,44]. In the electrically optimum situation, the thickness of $MoO_3$ used as HTL ($d_{id}$:$d_{MoO3}$) significantly affects the photovoltaic performance of the devices, and $d_{id}$=10 nm is extremely favorable for effective charge transport[8,14]. Therefore, $d_{id}$=10 nm was chosen for the OSCs investigated in this study.

In both opaque and semi-transparent OSC structures, Ag metal has been employed as the top electrode owing to its comparatively lower absorption coefficient and superior electrical conductivity compared to other common metals utilized in DMD systems and OSCs[22,36,37]. Oxidation of Ag is prevented by $WO_3$ in the asymmetric $MoO_3$/Ag/$WO_3$ transparent contact system[44]. Furthermore, the high refractive index of $WO_3$ enables it to serve as an efficient cap layer and waveguided for tunable optical features[15,44].

DMD transparent contact systems should be fine-tuned considering the application potential of integrated ST-OSCs. For ST-OSCs intended for window applications, it is desired that the DMD system provides optical properties with high AVT and color coordinates near the Planckian locus or D65 [14,29]. A neutral color and a high CRI are other design parameters targeted for ST-OSCs[8,14]. These exceptional optical features are associated with the refractive indices and extinction coefficients of whole structures constituting the ST-OSC. Moreover, there is a direct relation between the thicknesses of the bottom and top dielectric materials and the very thin metallic layer integrated with the DMD system. Therefore, for the ST requirement of PTB7-based OSCs, the AVT, CRI, and color features were evaluated through the integrated asymmetric $MoO_3$/Ag/$WO_3$ (10/$d_m$/$d_{od}$ nm) DMD transparent top contact system.

## The optical performance of PTB7-based ST-OSC with $MoO_3$/Ag/$WO_3$

The different features specified when selecting OSC structures have come to the forefront. The structure with maximum AVT ($AVT_{max}$), designed to have the highest optical transmittance in the visible region, represents one of the mentioned features. The other feature to be analyzed is the structure with the maximum $CRI_{ext}$, which was simulated in our previous study and fabricated in this study. This structure is referred to as $(CRI_{ext})_{max}$. In addition, without adding a new layer, the extreme point that can be reached in the chromaticity diagram for PTB7-based OSC with only DMD integration was determined by calculations and a structure called extreme color was fabricated to investigate this feature.

Within the scope of the current study, $AVT_{max}$, $(CRI_{ext})_{max}$ and Extreme Color structures, which were determined to be optimal with their different optical properties among 100 thousand solar cell structures previously modeled using TMM and then theoretically examined in detail in terms of their optical and electrical properties, were produced by going through the fabrication stages mentioned in detail in the Materials and Methods section. Similarly, opaque OSC, the conventional structure determined as the reference point of these structures, was also fabricated. In addition to the detailed calculations with TMM calculation, optical measurements were performed using UV-Vis spectrometry to compare the experimental results of the optimally determined structures.

Another objective of this study is to achieve color variation exclusively through the DMD system without resorting to alloying, doping, band modification, or integrating external photonic crystal systems. Due to the inherent optical properties of PTB7-based ST-OSCs, it is possible to produce colorless devices and to design

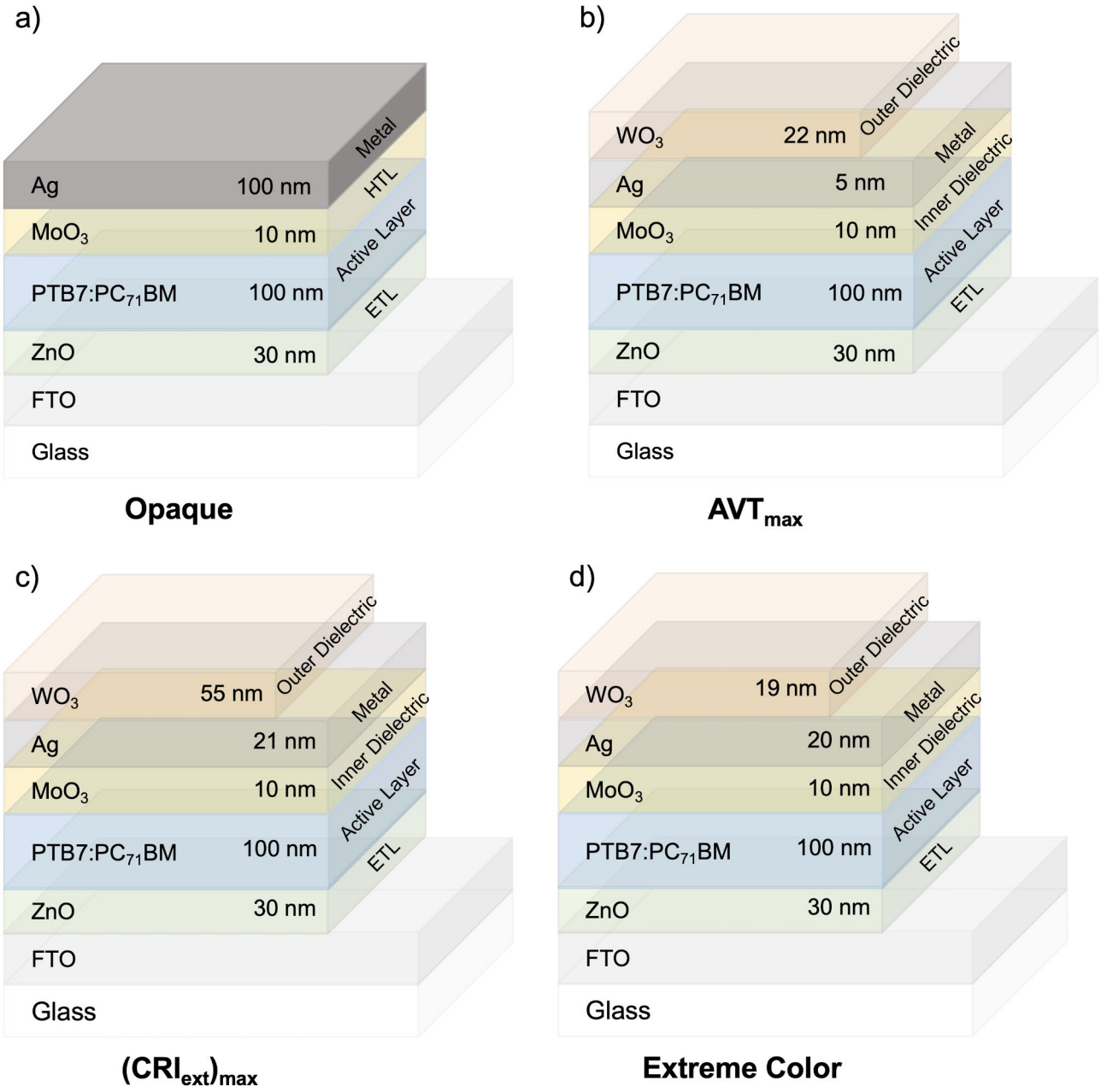



**Fig. 1**. PTB7-based (**a**) opaque organic solar cell, (**b**) semi-transparent organic solar cell having maximum AVT, (**c**) having maximum $CRI_{ext}$ and (**d**) having extreme color.

them solely in blue color without the need for photonic crystals. Thus, it is essential to identify the most extreme colors that can be achieved in PTB7-based ST-OSCs without modifying the cell structure through methods such as alloying, doping, interface modification, or band alignment. Consequently, an optical and photovoltaic comparison between the structures designed with Extreme Color and those designed to be colorless, such as $AVT_{max}$ and $(CRI_{ext})_{max,}$ is of significant importance. The transmittance measurement results of the optimally determined structures are given in Fig. 2. When the transmittance characteristics of the $AVT_{max}$ structure are examined, the calculation results are reflected in the experimental results. While the theoretical transmittance results are given with a dashed line, the experimental data are represented by a solid line.

The AVT calculated using TMM for the $AVT_{max}$ structure, which was 48.75%, was found to be 47.14% at the end of the calculations obtained from the experimental data. When the AVTs from experimental and theoretical results are compared, it is clear that they are compatible with one another. Similarly, for the $(CRI_{ext})_{max}$ and Extreme Color structures, it was observed that the experimental results are quite consistent with the calculation results made with TMM, and at the same time, the rate of change of these structures is similar when compared with each other.

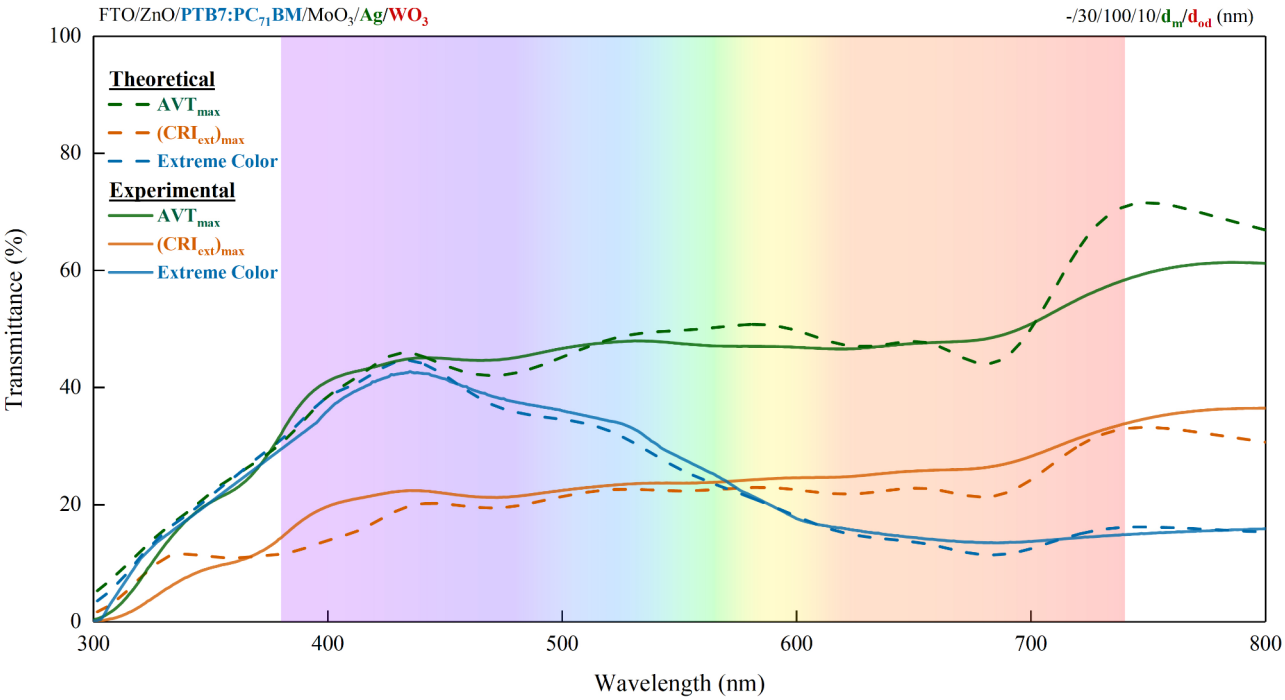



**Fig. 2**. Theoretical (from our previous study[13]) and experimental transmittance spectra of optimally designed PTB7-based ST-OSCs with outstanding optical performance.

It is important to determine the structure parameters of the PTB7-based OSC integrated with the asymmetric $MoO_3$/Ag/$WO_3$ (10/$d_m$/$d_{od}$ nm) DMD transparent contact system by determining the AVT as well as the color features and the variation of CIE1931 color coordinates. Even though AVT, which is examined especially for the ST objective, and $CRI_{ext}$, examined for color efficiency, are essential for lighting in-door applications, color features are crucial for exterior architecture and indoor lighting. This is because effective architectural and industrial designs should be made for AIPV and BIPV applications with ST-OSCs. The theoretical and experimental CIE x and y coordinates and $CRI_{ext}$ distributions calculated from the transmittance spectra of ST-OSCs performing optimal outstanding optical performance are given in Fig. 3a and b, respectively.

The DMD system of a PTB7-based ST-OSC can only be used to change color from neutral to blue region[13]. For the optimal structures provided for AVT and $CRI_{ext}$, the color coordinates are very close to each other and to the AM 1.5G color coordinates. Thus, a 'colorless' PTB7-based ST-OSC with neutral color perception can be achieved for industrial designs requiring high AVT and $CRI_{ext}$.

There are slight differences between the theoretically and experimentally obtained optical characteristics. This can be attributed to the thickness calibration, especially in the sputtering system, and the possibility that the layers forming the cell may deviate slightly from the targeted thicknesses. Furthermore, TMM is a calculation method that assumes that the thickness of each layer is homogeneous and the surface is smooth. In practice, the sputter system may deviate slightly from the thickness, and surface homogeneity and roughness may occur. This could be another reason for the slight discrepancy between experimental and theoretical results. Besides that, the chemical structure of the PTB7:$PC_{71}$BM blend active region is very sensitive to ambient conditions[45,46]. This may prevent the active region from being coated with the required thickness and homogeneity. These reasons could lead to slight differences between experimental and theoretical results[14]. When the AVT and CIE 1931 color coordinates in Table 1 are examined to see the difference in detail, it is seen that there is no significant discrepancy.

## Photovoltaic performances of PTB7-based ST-OSCs with $MoO_3$/Ag/$WO_3$

The current-voltage measurements were performed in darkness and under 1 sun to determine the photovoltaic performance of the optimally designed PTB7-based ST-OSCs with outstanding optical performance. The J-V and P-V results of all fabricated ST-OSC structures are given in Fig. 4. Examining the PCE result, one of the parameters determined experimentally from the J-V results, it is seen that the PCE, which is 7.6% for the opaque structure, decreased to 3.93% in the designed $AVT_{max}$ structure. For the structure with maximum AVT designed with TMM calculations, waiving the efficiency value to increase the optical transmittance is preferred with the light management engineering approach. This decrease is also predicted to occur in the external quantum efficiency (EQE) results for determining electrical properties with TMM[13]. The reduction in optical transmittance of the structure, or other words, the transition to an opaque state, is the most significant factor in increasing efficiency by harvesting more photons in the active region containing the PTB7:$PC_{71}$BM blend.

The FF evaluation was found to be in the range of 65-70% for optimally designed PTB7-based.

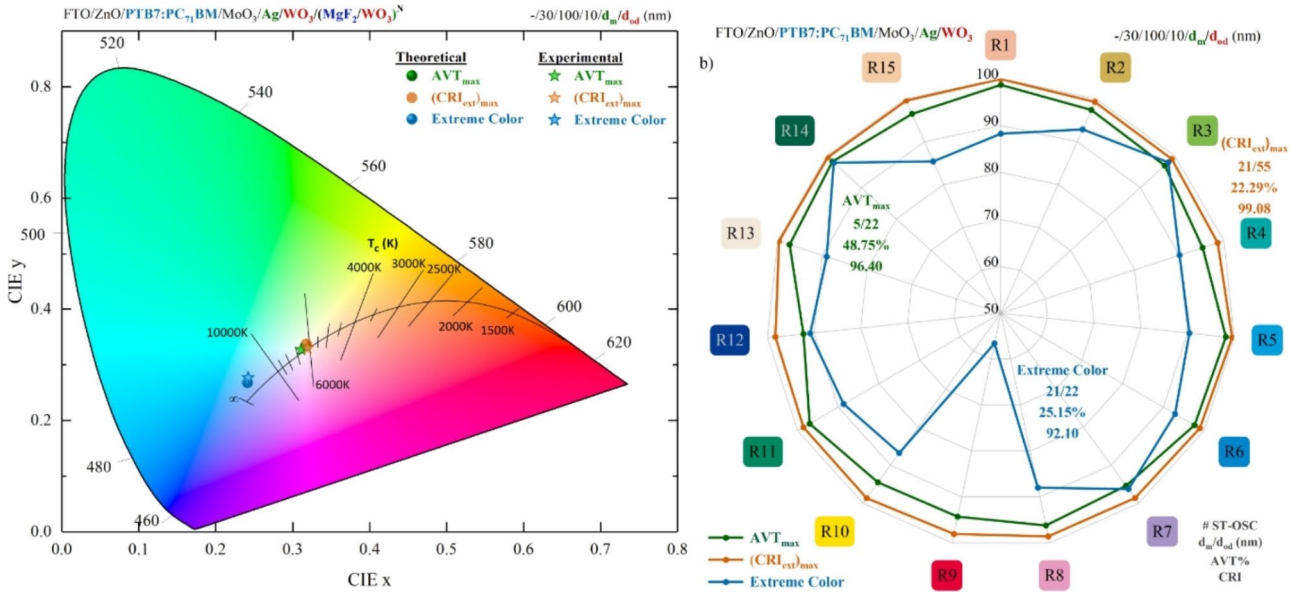



**Fig. 3**. Comparison of the optical performance (**a**) experimentally and theoretically (from our previous study[13]) obtained color coordinates and (**b**) TCS values for $AVT_{max}$, $(CRI_{ext})_{max}$ and Extreme Color of optimally designed PTB7-based ST-OSCs.

| ST-OSC | Theoretical | | | | Experimental | | | |
|---|---|---|---|---|---|---|---|---|
| | AVT (%) | $CRI_{ext}$ | CIE x | CIE y | AVT (%) | $CRI_{ext}$ | CIE x | CIE y |
| $AVT_{max}$ | **48.75** | 96 | 0.32 | 0.33 | **47.14** | 95 | 0.31 | 0.33 |
| $(CRI_{ext})_{max}$ | **22.29** | 99 | 0.32 | 0.34 | **23.82** | 97 | 0.32 | 0.33 |
| Extreme Color | **25.15** | 92 | 0.24 | 0.27 | **26.34** | 90 | 0.24 | 0.28 |

**Table 1**. Theoretical (from our previous study[13]) and experimental comparison of optical parameters for optimally designed PTB7-based semi-transparent organic solar cells with outstanding optical performance. Significant values are in bold.

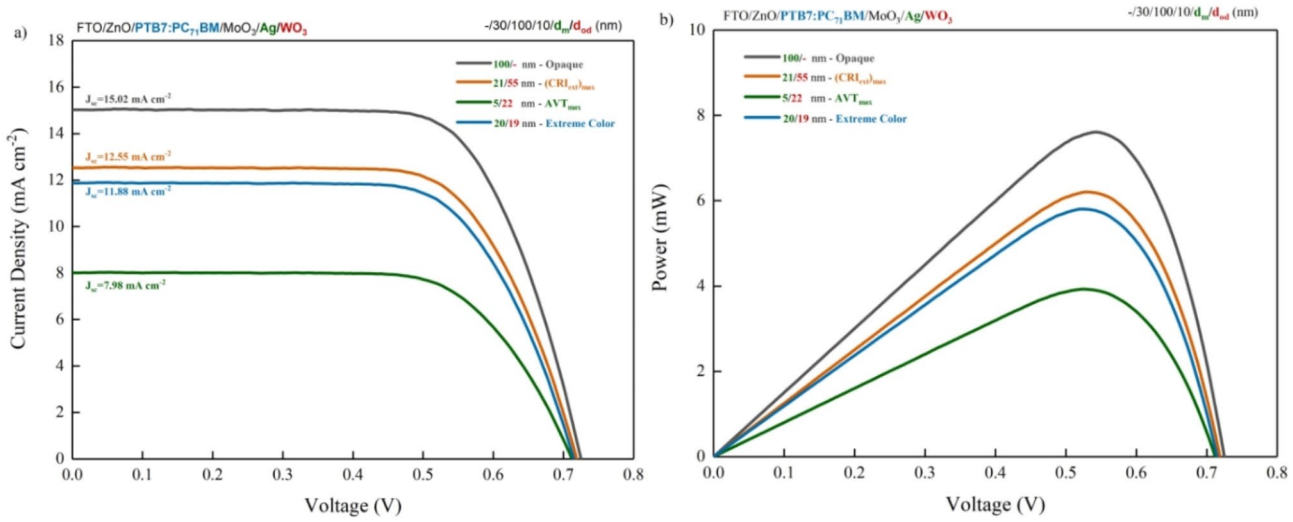



**Fig. 4**. Comparison of (**a**) J-V and (**b**) P-V characteristics of opaque, $AVT_{max}$, $(CRI_{ext})_{max}$, and Extreme Color structures of optimally designed PTB7-based ST-OSCs with outstanding optical performance.

ST-OSCs exhibit all outstanding optical performance. This result agrees with other studies in the literature for PTB7-based structures[1,19,20]. In addition, the structures' band arrangement and contact materials are identical. This situation does not lead to a significant change in $V_{oc}$, $V_m$ and $J_m$. Because $V_{oc}$ mainly depends on the difference in the work function of the metal contacts. If an ohmic contact is formed in the electrodes, $V_{oc}$ depends on the HOMO–LUMO difference of the donor and acceptor materials forming the active region[2]. $V_m$ is directly dependent on $V_{oc,}$ so the band gap, recombination rates, absorption characteristics and contact structures are effective on $V_m$. $J_{sc}$ represents the number of charge carriers generated and eventually collected in the active region under short circuit conditions. The small band gap, the high absorption coefficient of the active region, smaller phase separation, and high carrier mobility of the layers, such as ETL and HTL that form the solar cell improve $J_{sc}$[2]. Increasing the absorption characteristics with various DMD modifications in the cell structure or integration, such as photonic crystal, can improve $J_{sc}$. In all the ST-OSC architectures designed and produced in the study, only the thicknesses of $MoO_3$/Ag/$WO_3$, which is the top contact, are different, and their absorption characteristics are modified. In all cell architectures, the bottom contact, ETL, active region, HTL and top contact material are the same; therefore, the band arrangements are the same. Therefore, since the main cell structure, except for the $MoO_3$/Ag/$WO_3$ DMD transparent contact system, is the same in the cell architectures, an improvement in absorption affects $J_{sc}$. Since the band arrangement is the same, no significant change is observed in $V_{oc}$ and $V_m$.

The experimental results show that the $J_{sc}$ of the structures are ranked similarly to the theoretical calculations. The opaque structure, which has the highest photon harvest, produces the highest current density, as expected. Extreme Color and $(CRI_{ext})_{max}$ structures are also ranked in the EQE results and measured as 11.88 mA/cm$^2$ and 12.55 mA/cm$^2$, respectively. When the P-V results are analyzed in Fig. 4b, a similar ranking can be mentioned, and again, the results are as expected from the calculations.

Short circuit current density of $AVT_{max}$, Extreme Color and $(CRI_{ext})_{max}$ are also ranked in the EQE results and found to be 7.98 mA/cm$^2$, 11.88 mA/cm$^2$, and 12.55 mA/cm$^2$ from J-V measurements, respectively. The consistency between the EQE and $J_{sc}$ changes can also be seen in the cells' experimental and theoretical transmittance spectra. The transmittance of $(CRI_{ext})_{max}$ is relatively lower in a wide wavelength range, indicating that the structure's absorption characteristics are relatively better. Therefore, the photon harvesting is improved by increasing the absorption, and the highest $J_{sc}$ is obtained in the $(CRI_{ext})_{max}$. In the Extreme Color, since blue color can be obtained, the transmittance is low, especially in the short wavelength regime in the visible region and high in long wavelength. This situation keeps the absorption at a more average value than other structures, decreasing the photon harvesting in short wavelengths and enhancing it in long wavelengths. Therefore, the Extreme Color obtains a relatively average $J_{sc}$. Theoretical and experimental results, including photovoltaic performance parameters obtained from current-voltage measurements for Opaque, $AVT_{max}$, $(CRI_{ext})_{max}$ and Extreme Color structures, are given in Table 2.

Considering OSC structures, although the decrease in the PCE creates a disadvantage for a device that converts electromagnetic energy into electrical energy, increasing the transmittance properties by waiving the efficiency at the lowest possible rate to add a semi-transparent feature creates different advantages. For this reason, the results obtained to demonstrate the compatibility of TMM computation and experimental results are of great importance for the devices to be constructed by designing the structures with various advantages and engineering them in accordance with the required purposes.

When the experimental AVT and PCE for $AVT_{max}$, which is designed with light management engineering and optimized for maximum visible transmittance and efficient photon harvesting, are compared to the values obtained in structures with similar top contact structures in the literature, it is clear that the study achieves very optimal photovoltaic performance. Therefore, it is imperative to determine the structure parameters that provide efficient photon harvesting and maximize the efficiency in the cell architecture where the maximum AVT is obtained with light management engineering. In particular, 47% AVT and 3.0% PCE were obtained in the cell designed with $MoO_3$/Mg/Ag/$MoO_3$ anode/HTL by Zheng et al.[28]. The highest recorded PCE has been found in a study by Xu et al.[19] at 6.4%. However, AVT is relatively low in the building architecture used in the same study, with a value of 16.9%. In the study discussed here, the highest AVT in the literature was achieved in the cell structure presented with the $AVT_{max}$ structure architecture, while at the same time, a PCE of 3.9% was obtained. The PCE is increased by 30% compared to those achieved in architectures with the same AVT and a similar anode/HTL. This shows that a very high photon harvesting is also achieved with efficient visible light transmission, and the methodology motivated in this study has emerged as a crucial design method.

| | Theoretical | Experimental | | | | | |
|---|---|---|---|---|---|---|---|
| ST-OSC | $J_{sc}$ (mA/cm$^2$) | $V_{oc}$ (V) | $J_{sc}$ (mA/cm$^2$) | $V_m$ (V) | $J_m$ (mA/cm$^2$) | PCE (%) | FF (%) |
| Opaque | **16.16** | 0.725 | **15.02** | 0.542 | 14.04 | **7.61** | 69.9 |
| $AVT_{max}$ | **9.88** | 0.710 | **7.98** | 0.528 | 7.44 | **3.93** | 69.1 |
| $(CRI_{ext})_{max}$ | **13.64** | 0.719 | **12.55** | 0.527 | 11.77 | **6.21** | 69.0 |
| Extreme Color | **13.06** | 0.715 | **11.88** | 0.525 | 11.06 | **5.81** | 68.3 |

**Table 2**. Photovoltaic performance parameters for Opaque, $AVT_{max}$, $(CRI_{ext})_{max}$ and Extreme Color structures of optimally designed PTB7-based ST-OSCs with outstanding optical performance. Significant values are in bold.

## Bifaciality performance of PTB7-based ST-OSCs with $MoO_3$/Ag/$WO_3$

In the scope of this study, the bifacial properties of semi-transparent solar cell structures have been investigated to take advantage of their outstanding optical performance properties and the advantages of the structure architecture that allows bilateral light entry into the cells. Bifacial solar cells are structures that aim to collect reflected photons and photons incident on the structure from one side. Using a bifacial configuration that can harvest energy from both the rear and front surfaces is a convenient way to increase the utilization of sunlight[47].

In contrast to monofacial SCs, bifacial SCs entail numerous design prerequisites. Foremost among these is the seamless incorporation of transparent top contact and HTL structures within the cell architecture, facilitating effective light ingress from the rear surface to the active region. Similarly, the active region thicknesses should not be too high, and the use of thin film active layers or polymers is necessary for efficient bifacial cell properties. Besides, the active region of the organic solar cell is in the bulk heterojunction structure formed by blending organic semiconductors acting as donors and acceptors. In this respect, the bulk heterojunction forms a much larger heterojunction interface distributed throughout the entire layer. Thus, it is more efficient that all molecules are within the diffusion length and the electrons and holes generated by photoexcitation are collected by the internal electric field. Therefore, it does not matter from which direction the light enters the organic solar cell in the bulk heterojunction structure. For inorganic semiconductors, it is crucial that the light enters from the p- or n-type side since it forms the active region of the p- and n-type materials, located in spatially different regions that are not mixed and grown layer by layer. In particular, the rapid absorption of light near the surface where it enters the structure affects how much the electric field will be felt by the carriers produced. For all these factors, the bifacial performance of organic solar cells that can be designed in bulk heterojunction structure is considerably higher than that of inorganic-based solar cells that can be grown layer by layer.

The cells designed as semi-transparent with a bulk heterojunction active region examined in the study are potentially used as bifacial structures. Besides the fact that the active region thickness is not high, dielectric materials and thin metal layers used as anti-reflection layers for high transmittance are of great importance for the bifaciality feature. That is why the investigation of the bifaciality properties of the cells is suitable for currently designed solar cells. The bottom and top illumination are shown in Fig. 5a. For inverted structures, where the light enters the solar cell from the bottom, examining the top illumination results and comparing these results are of paramount importance for determining the bifaciality properties. For this reason, the comparison of reflectance and absorption spectra under bottom and top illumination for $AVT_{max,}$ $(CRI_{ext})_{max}$ and Extreme Color structures are given in Fig. 5b and c, respectively.

Analyzing the reflectance spectrum for the $AVT_{max}$ structure, it is noteworthy that the difference between the theoretical and experimental values is very low. The fact that the reflectance spectrum takes close and low values in both top and bottom illumination shows the potential of the $AVT_{max}$ structure to operate as bifacial. For $(CRI_{ext})_{max}$ and Extreme Color structures, it was observed that there was a difference between the intensities of the reflectance spectra in the bottom and top illumination. Similar to the results seen in the reflection spectrum, extremely similar outcomes were observed in the absorption spectrum for the $AVT_{max}$ structure in the bottom and top illumination. $(CRI_{ext})_{max}$ and Extreme Color structures exhibit a different distribution of absorption spectra, especially in the visible region.

As the direction of light entering the solar cell varies, the electric field distribution is also affected along with the optical properties. The change of the first layer that the incident electromagnetic wave will encounter with the change of the direction of illumination of the structures designed as ST-OSC will have a similar effect on the electric field distribution by changing the reflection and absorption spectra. For $AVT_{max}$, $(CRI_{ext})_{max}$ and Extreme Color structures, the comparative results of the electric field distribution in the bottom illumination with the electric field distribution in the top illumination are presented in Fig. 6a, b and c, respectively.

Comparing the electric field distributions in the top and bottom illumination for the $AVT_{max}$ structure, it is possible to mention that they have similar distributions. The electric field distribution is observed to reach the active region at similar ratios, especially for the visible region. When the absorption and reflection spectra in the upper part of Fig. 6 are analyzed, they show similar distributions. With this result, based on the similar distributions of electric field distribution and absorption spectra for top and bottom illumination, photovoltaic performances are expected to show close results.

For the $(CRI_{ext})_{max}$ structure of the ST-OSCs, which was designed as inverted and the bottom illumination analyses were performed in the previous section, the electric field distribution as a result of the top illumination shows differences. It was observed that the electric field was prevented from penetrating the structure by the effect of Ag metal with a thickness of 21 nm in nearly the entire visible region. The increase in reflectivity in a wide wavelength region with increasing metal thickness resulted in the electromagnetic wave not reaching the active region and decreased absorption. The Ag metal layer, which encounters the electromagnetic wave at the end in the bottom illumination and increases the photon harvesting with its reflectance, negatively affects the photon harvesting by preventing the photons from entering the structure with its reflectance, this time with the top illumination. Ag, which contributes to the electric field distribution, especially in the IR region with its reflectance, causes the electric field distribution in the IR region to remain lower in the case of top illumination. With the decrease in the intensity of the electric field distribution in the active region in the top illumination and the absorption remaining low, photovoltaic performance loss is expected for the $(CRI_{ext})_{max}$ structure. For the $(CRI_{ext})_{max}$ structure, which exhibits excellent photovoltaic properties in the bottom illumination, the decrease in photovoltaic performance adversely affects the bifacial properties.

Looking at the difference between the top and bottom illuminations of the electric field distribution for the Extreme Color structure, we observe a change due to the effect of Ag metal thickness similar to the $(CRI_{ext})_{max}$ structure. The Ag metal, which is 21 nm in the $(CRI_{ext})_{max}$ structure, has caused a similar effect with a thickness of 20 nm for Extreme Color. Particularly in the IR region, the electromagnetic wave is prevented from entering the structure due to the reflectivity of Ag metal.

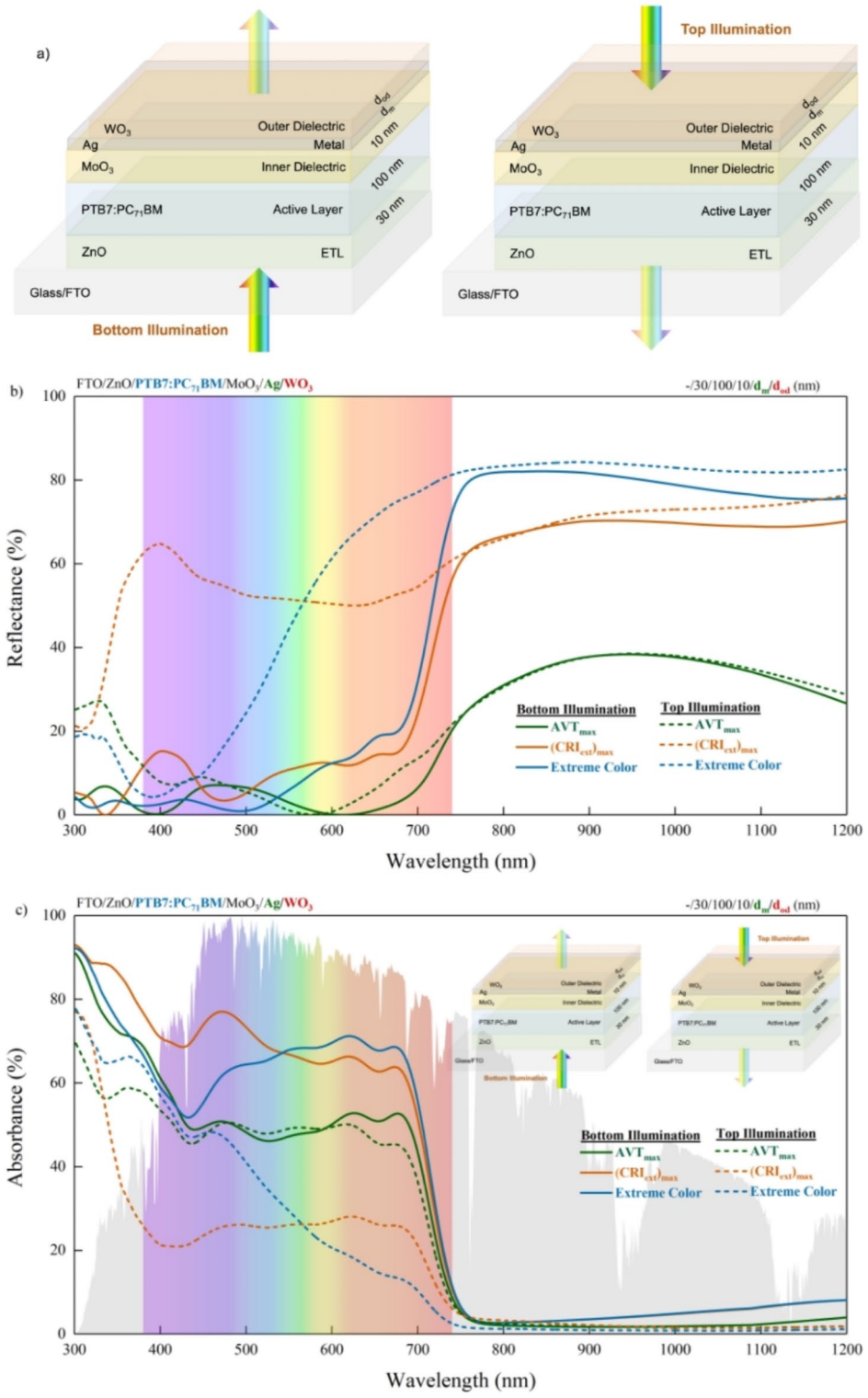



**Fig. 5**. Optimally designed PTB7-based ST-OSCs exhibit outstanding optical performance, including (**a**) bottom and top illumination, (**b**) reflectance and (**c**) absorbance spectra.

The EQE and quantum utilization efficiency (QUE) results determined with TMM, in addition to the optical spectra, should be analyzed theoretically in order to evaluate the photovoltaic properties. Thus, the EQE and QUE results of $AVT_{max}$, $(CRI_{ext})_{max}$ and Extreme Color structures are presented in Fig. 7a and b.

When the EQE results are examined, it is possible to mention almost identical spectra for the $AVT_{max}$ structure in the top and bottom illumination. This result again shows the importance of the $AVT_{max}$ structure in showing a bifacial feature in accordance with the optical spectra examined. The $J_{sc}$ obtained from EQE calculations was

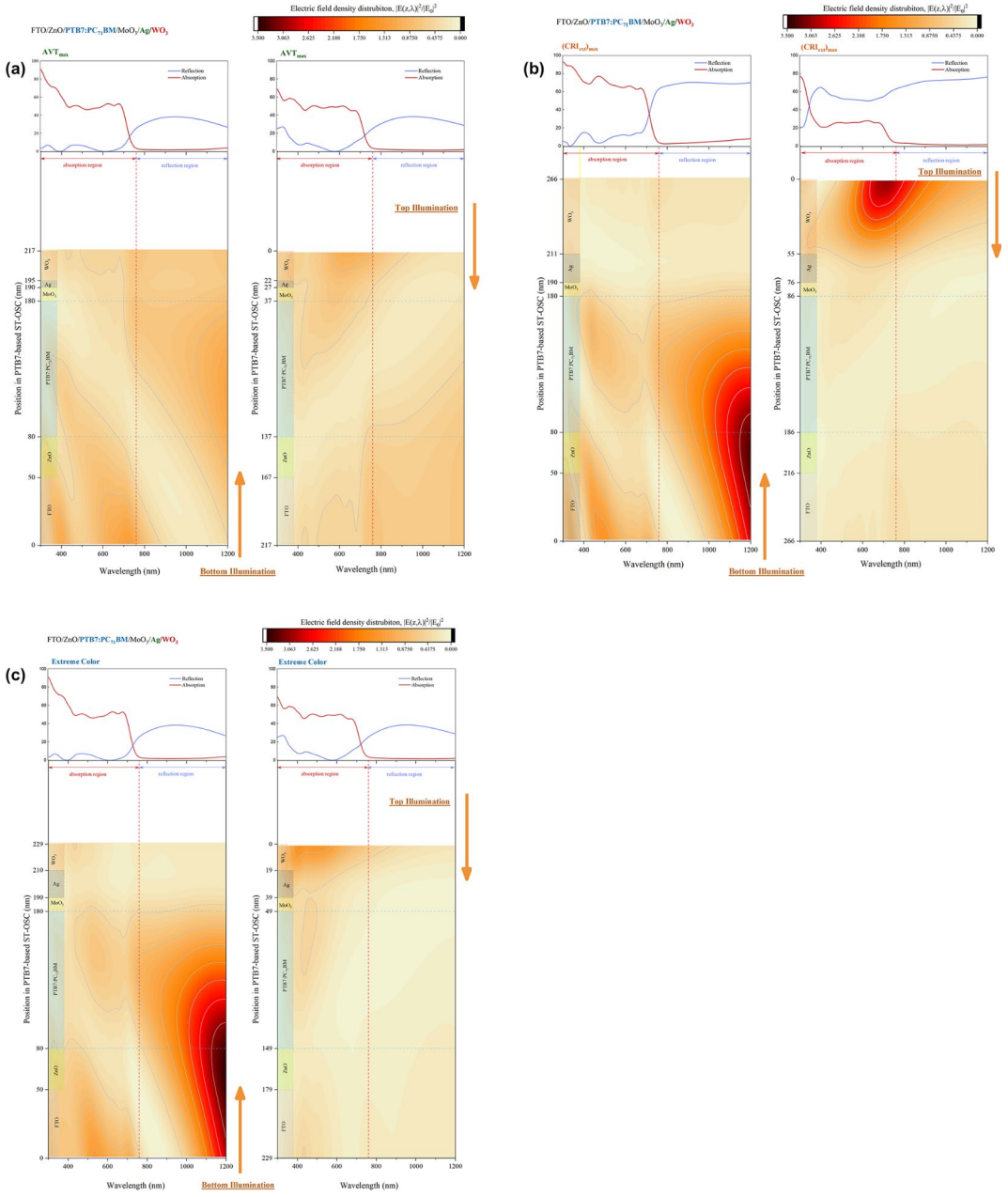



**Fig. 6**. Wavelength and position-dependent electric field density distributions of (**a**) $AVT_{max}$, (**b**) $(CRI_{ext})_{max}$ and (**c**) Extreme Color at bottom and top illumination.

found to be 9.88 mA/cm$^2$ for bottom illumination and 9.53 mA/cm$^2$ for top illumination. It was observed that the $J_{sc}$ took nearby values in accordance with the EQE change. This situation emphasizes the $AVT_{max}$ structure for the potential of the bifacial solar cell.

The EQEs of $(CRI_{ext})_{max}$ and Extreme Color structures are examined in the top and bottom illuminations and it is seen that there are differences in terms of intensity and distribution. For the $(CRI_{ext})_{max}$ structure, the $J_{sc}$ was calculated as 13.64 mA/cm$^2$ in the bottom illumination and 4.34 mA/cm$^2$ in the top illumination. For Extreme Color, the $J_{sc}$ was 13.06 mA/cm$^2$ in the bottom illumination and 4.37 mA/cm$^2$ in the top illumination. $J_{sc}$ results found theoretically with TMM and $AR_{AM1.5G}$ results, which express the reflection from AM1.5G irradiance, are presented in Table 3 to see the differences in the bottom and top illumination.

Comparing the QUE results, it is possible to state that similar changes are observed in the EQE results. Considering that one of the parameters affecting the QUE result is EQE and the other is.

T (transmittance), and since it is known that the top and bottom illumination for T does not show the exact change for these transparent structures, it is inevitable that the EQE result is a direct determinant of the QUE result. For this reason, like the EQE result, while the QUE curves of the $AVT_{max}$ in the top and bottom

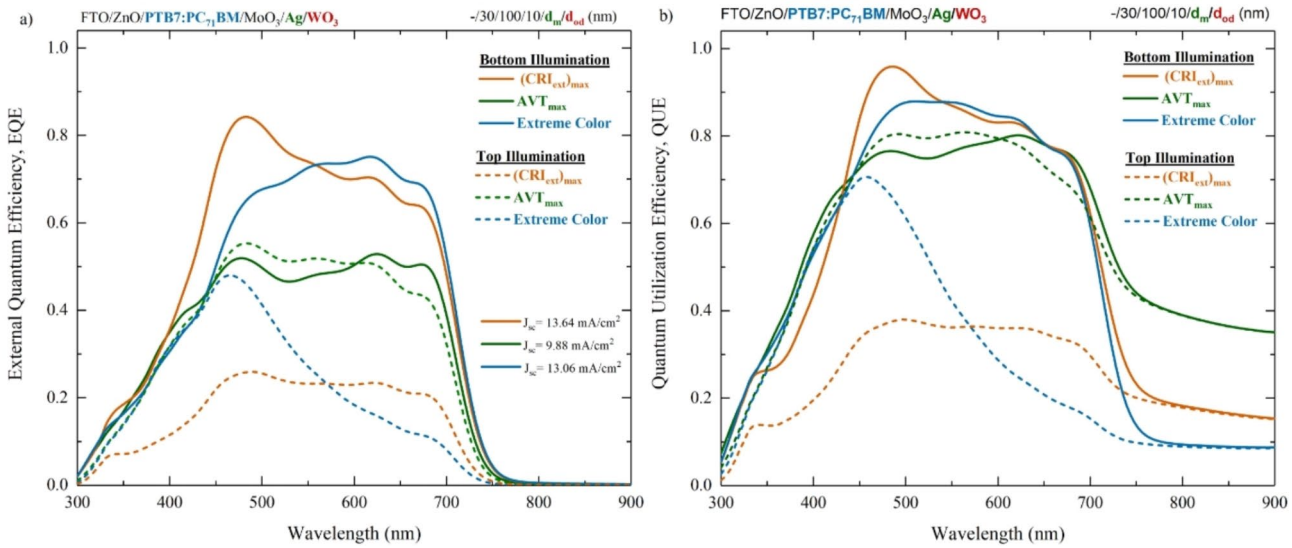



**Fig. 7**. Characteristics of (**a**) EQE and (**b**) QUE in the bottom and top illumination of ST-OSC.

| ST-OSC | Illumination | $AR_{AM1.5G}$ (%) | $J_{sc}$ (mA/cm²) |
|---|---|---|---|
| $AVT_{max}$ | Bottom | **15.15** | **9.88** |
| | Top | **17.16** | **9.53** |
| $(CRI_{ext})_{max}$ | Bottom | 33.63 | 13.64 |
| | Top | 59.79 | 4.37 |
| Extreme Color | Bottom | 37.39 | 13.06 |
| | Top | 57.82 | 5.27 |

**Table 3**. Theoretical $AR_{AM1.5G}$ and $J_{sc}$ of ST-OSC structures in the bottom and top illumination. Significant values are in bold.

illumination give similar results, it is seen that the QUE intensity changes for $(CRI_{ext})_{max}$ and Extreme Color structures.

Analyzing the $AR_{AM1.5G}$ results for the $AVT_{max}$, it is noteworthy that the reflection of AM1.5G is close to each other in the top and bottom illumination. $AR_{AM1.5G}$, which was 15.15% in the bottom illumination, took 17.16% in the top illumination. The close and low values of the reflection will directly affect the photovoltaic performance and, therefore, the bifaciality feature. Thanks to the anti-reflective feature of the asymmetric $MoO_3$/Ag/$WO_3$ DMD structure, which was optimal for the $AVT_{max}$, the low reflection feature provided an advantage for bifaciality. When we look at the $AR_{AM1.5G}$ results for $(CRI_{ext})_{max}$ and Extreme Color, the difference between bottom and top illumination was encountered. The DMD structure loses its anti-reflective property due to the effect of Ag metal and takes different values in bottom and top illumination.

In the framework of the study, the 1 solar bottom illumination I-V results of the ST-OSCs were also analyzed with the same parameters for the top illumination analysis. Photovoltaic performance parameters for $AVT_{max}$, $(CRI_{ext})_{max}$ and Extreme Color were determined as a result of the I-V measurements conducted in bottom and top illumination. J-V and P-V results obtained from the I-V results for $AVT_{max}$, $(CRI_{ext})_{max}$ and Extreme Color structures in the top illumination are given in Fig. 8a and b, respectively.

Analyzing the J-V curves for the $AVT_{max}$ structure, it is seen that the results are close to each other in the bottom and top illumination. This situation does not directly affect the efficiency calculated from I-V measurements and can be recognized from the P-V curve. As can be seen from Table 4, the PCE is 3.93% and 3.67% for the $AVT_{max}$ structure in the bottom and top illumination, respectively. The bifaciality factor, calculated by the ratio of the PCEs in the bottom and top illuminations, was determined as 0.94, with the effect of the PCEs being close to each other. For the $AVT_{max}$ structure, it is determined that the target of high transmittance in the visible region positively affects the bifacial feature.

Examining the J-V and P-V results of the $(CRI_{ext})_{max}$ structure, the difference arising from the effect of metal thickness and also encountered in the optical results was observed. As can be seen in Table 4, with the difference seen between the J-V and P-V curves in the bottom and top illumination, PCE has taken values of 6.21% and 1.58% for the bottom and top illumination, respectively. Consequently, the bifaciality factor was found to be 0.25. Similar situations to the $(CRI_{ext})_{max}$ structure can be mentioned when the Extreme Color is evaluated. In particular, it can be mentioned that the bifaciality feature is lower due to the thicker reflective layers compared to the $AVT_{max}$ structure. Analyzing the J-V and P-V results, it was observed that the curves were far from each

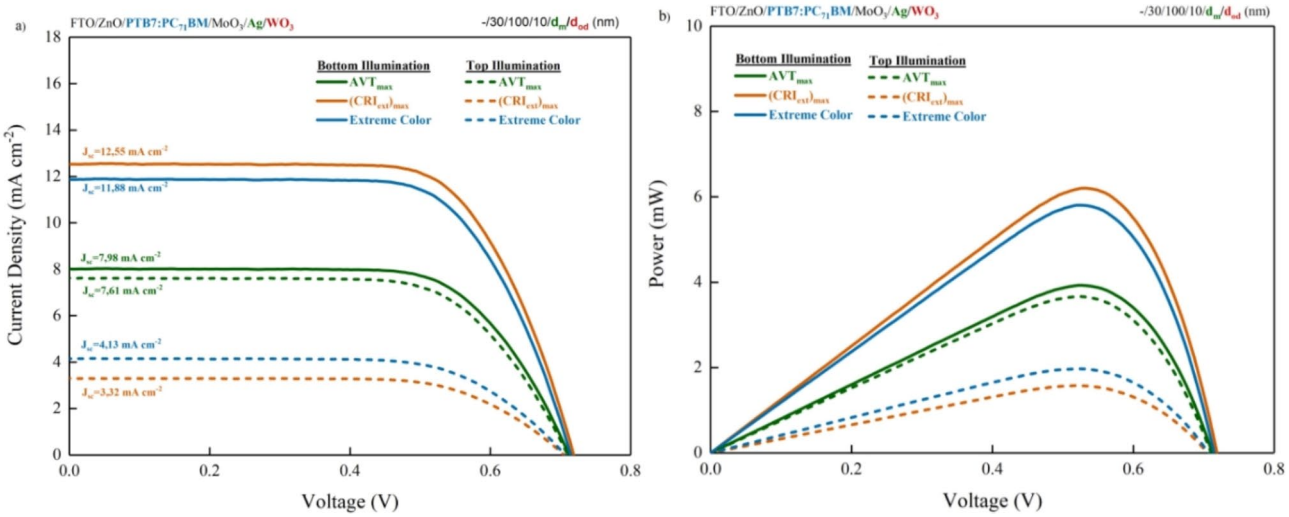



**Fig. 8**. Comparison of (**a**) J-V and (**b**) P-V characteristics of bifacial ST-OSC structures.

| ST-OSC | Illumination | $V_{oc}$ (V) | $J_{sc}$ (mA/cm$^2$) | $V_m$ (V) | $J_m$ (mA/cm$^2$) | FF (%) | PCE (%) | Bifaciality |
|---|---|---|---|---|---|---|---|---|
| $AVT_{max}$ | Bottom | 0.710 | 7.98 | 0.528 | 7.44 | 69.1 | **3.93** | **0.94** |
| | Top | 0.709 | 7.61 | 0.524 | 7.01 | 68.1 | **3.67** | |
| $(CRI_{ext})_{max}$ | Bottom | 0.719 | 12.55 | 0.527 | 11.77 | 69.0 | **6.21** | **0.25** |
| | Top | 0.702 | 3.32 | 0.520 | 3.04 | 67.7 | **1.58** | |
| Extreme Color | Bottom | 0.715 | 11.88 | 0.525 | 11.06 | 68.3 | **5.81** | **0.34** |
| | Top | 0.705 | 4.13 | 0.522 | 3.77 | 67.7 | **1.97** | |

**Table 4**. Photovoltaic performance parameters of bifacial ST-OSC structures under bottom and top illumination. Significant values are in bold.

other in the bottom and top illumination. As a result, the calculated PCE was 5.81% for bottom illumination and 1.97% for top illumination. Consequently, the bifaciality factor was calculated as 0.34 due to the difference between the PCEs in different illuminations.

Fujii et al.[48] found that for the DMD integrated OSC with active region PTB7:$PC_{71}BM$ and Au metal, the PCE was 3.1% in the bottom illumination and 2.1% in the top illumination, and the bifaciality factor was 0.68. In the same study, the PCE for DMD-integrated OSC using Ag metal was 2.9 in the bottom illumination and 1.3 in the top illumination, and the bifaciality factor was 0.45 [48]. The bifaciality factor obtained for the $AVT_{max}$ structure examined in this study is significant in showing the bifaciality potential of such a structure. Considering that the bifaciality factor will be the highest when it is closest to 1, it will be possible to conclude that the TMM calculation and the fabrication method utilized in the study are critically important for determining and obtaining structures with bifacial properties.

There are many studies on bifaciality for inorganic solar cells, especially for Si-based solar cells[49]. Böscke et al. showed that the bifaciality factor 0.98 for Si-based cells was obtained with PCEs around 20%[50]. Subedi et al. obtained a bifaciality factor of 0.53 for CdTe-based solar cells by varying the absorber layer thickness[51]. Likewise, in the study conducted by Çetinkaya, a bifaciality factor of 0.46 was obtained for CdTe-based solar cells[17]. Nishimura et al. obtained a bifaciality factor of 0.91 for CIGSe solar cell structure for PCE around 23%[52]. Compared to inorganic solar cells, it is possible to mention that among the organic solar cell structures examined in this study, the $AVT_{max}$ structure will have an essential role in the literature with its high bifaciality properties.

## Conclusion

In this study, we have optimally designed and fabricated PTB7:$PC_{71}BM$ semi-transparent organic solar cells with high optical performance by integrating $MoO_3$/Ag/$WO_3$ asymmetric DMD system and presented an in-depth investigation of optical and photovoltaic properties. As an output of this study, the structure architectures with maximum AVT and maximum $CRI_{ext}$ for PTB7:$PC_{71}BM$ ST-OSC with $MoO_3$/Ag/$WO_3$ asymmetric DMD top contact have been determined. In addition, without integrating a new photonic-based system into the structure, the most extreme color architecture that can be achieved for a PTB7:$PC_{71}BM$ ST-OSC has been determined and fabricated. In addition to all these investigations, the bifaciality properties of the fabricated PTB7-based ST-OSCs were analyzed, and the structure architecture with the highest bifaciality was determined.

In PTB7:$PC_{71}BM$ ST-OSC, the maximum AVT is obtained for the $MoO_3/Ag/WO_3$ ($10/d_m/d_{od}$ nm) DMD for $d_m$=5 nm and $d_{od}$=22 nm and is 47.14%. For this design, PCE is 3.93%, and FF is 69.1%. The AVT of the structure to be designed with the optimal thickness values offers a very high AVT compared to the PTB7-based ST-OSCs in different structures with high AVT obtained in the literature. With the $MoO_3/Ag/WO_3$ DMD integration, the architecture with maximum CRI for PTB7:$PC_{71}BM$ ST-OSC was possible for $d_m$=21 nm and $d_{od}$=55 nm. In this design, CRI is 97, PCE is 6.21% and FF is 69%. It was also observed that the $MoO_3/Ag/WO_3$ DMD system has no bearing on the color rendering of PTB7-based ST-OSC and has high optical transmittance. Without utilizing any photonic system, we have identified a structured architecture for a PTB7:$PC_{71}BM$ ST-OSC by integrating a $MoO_3/Ag/WO_3$ DMD, where the color can be changed towards the extremes in the blue region. This structure's CIE x and y values are 0.2410 and 0.2683 for $d_m$=20 nm and $d_{od}$=19 nm, respectively. The structure with the most extreme blue color has a PCE of 5.81% and FF of 68.3%, with an AVT of 26.34 and a CRI of 90. In addition to achieving high optical performance, integrating the $MoO_3/Ag/WO_3$ DMD has given the PTB7:$PC_{71}BM$ ST-OSC the potential to be used as a double-sided device. For the building architecture offering maximum AVT, the bifaciality parameter was observed as 0.94. Thus, with the integration of the $MoO_3/Ag/WO_3$ asymmetric DMD system, the highest bifaciality value was obtained for PTB7:$PC_{71}BM$ ST-OSC.

Consequently, this study highlights the importance of precise control over the thickness and composition of the DMD layers to achieve the desired optical characteristics, such as color neutrality and high CRI. The findings suggest that with further optimization, these ST-OSCs could be highly effective in modern architectural applications, contributing to the development of energy-efficient, aesthetically pleasing buildings. The results demonstrate ST-OSCs' promising potential for applications in BIPV and other areas where transparency and energy conversion efficiency are critical.

## Material and method

### Calculation of optical spectra

The optical spectra, including absorption, transmittance and reflectance of PTB7-based ST-OSCs based on $MoO_3/Ag/WO_3$ ($10/d_m/d_{od}$ nm) DMD transparent top contact system have been investigated. The analysis is performed using the Transfer Matrix Method, which is well known for its efficiency in the simulation of optoelectronic devices. TMM is adept at studying the propagation of electromagnetic waves within a structure and theoretically determining their optical properties, especially in complex configurations such as DMD and photonic crystal architectures where multiple dielectric layers are stacked[14]. Detailed methodologies and equations used in TMM calculations are described in our previous research[13].

### Average visible transmittance

The transmission characteristics of semi-transparent optoelectronic systems are evaluated using AVT values, which are derived from transmittance spectra within the visible light wavelength range (370–740 nm), considering the photopic response of the human eye. AVT calculations involve the transmittance spectra analysis of PTB7-based ST-OSCs featuring the designed $MoO_3/Ag/WO_3$ DMD transparent top contact system, computed using the TMM.

### Calculation of CIE 1931 color coordinates

In addition to AVT, another crucial characteristic of ST-OSCs is defined by their color coordinates ($x$, $y$) within the CIE 1931 chromaticity diagram. This diagram, based on the human eye's photopic response, is extensively utilized for determining the color properties of illuminants. The methodology and equations employed in calculating the CIE 1931 color coordinates of PTB7-based ST-OSCs featuring the $MoO_3/Ag/WO_3$ DMD transparent top contact system are thoroughly elaborated upon in our previous publication[13].

### Color rendering index

Color rendering measures how accurate an object's color is when illuminated by an optimal or natural light source[29]. Therefore, CRI constitutes a measurement system that determines whether the colors of illuminated objects are accurate to the original and takes values in the range of 0-100. A CRI of 100 can be seen in standardized daylight sources or incandescent lamp bodies. CRI values of 90 and above are considered excellent, while CRI values below 80 are generally recognized as poor[13]. The method and equations used in calculating the CIE values of PTB7-based ST-OSCs with $MoO_3/Ag/WO_3$ DMD transparent top contact system are given in our previous study[13].

### External quantum efficiency and quantum utilization efficiency

The external quantum efficiency is intimately linked to the absorption of individual photons within the solar cell and the availability of electrons and holes that can contribute to the external circuit. The ratio of the electron flux from the SC to the incident photon flux determines it. The calculation of the EQE involves considering factors such as the distribution of the electric field intensity inside the SC and the optical properties of the materials involved, as detailed in our previous study[13]. The method and equations used to calculate EQE and QUE characteristics of PTB7-based ST-OSCs with $MoO_3/Ag/WO_3$ DMD transparent top contact system are given in our previous study[13].

### Experimental details

Within the scope of this study, the active regions of PTB7-based ST-OSCs with $MoO_3/Ag/WO_3$ ($10/d_m/d_{od}$ nm) DMD transparent top contact system are formed by a PTB7:$PC_{71}BM$ blend. The fabricated ST-OSCs have inverted device architecture with BHJ active region type. Chlorobenzene (chlorobenzene, CB) and 1,8-diiodoctane (1,8-diiodoctane, DIO), the solvents of both materials, were used to prepare the PTB7:$PC_{71}BM$

mixture. For the mixture used as a solvent, 970 mL CB and 30 mL DIO solution were mixed for 1 h. It was observed that DIO added chlorobenzene solution, which provided better surface adhesion and better efficiency for the PTB7:$PC_{71}BM$ blend[53]. Ho et al. observed that the ratio of DIO added to chlorobenzene ranged from 0 to 10%, and adding 3% gave the best result[53]. For this reason, the solvent was prepared by choosing a 97:3 ratio for the CB-DIO solution. To 1 mL of CB-DIO (97:3% by volume) solution, 10 mg of PTB7 and 15 mg of $PC_{71}BM$ were added, and the resulting 25 mg mixture of PTB7:$PC_{71}BM$ (1:1.5 by weight) was mixed with a magnetic stirrer at constant temperature for ~ 18 h 70 °C for homogeneity.

The spin coating technique was used in all film coatings to coat the active region. The results of the PTB7:$PC_{71}BM$ (donor: acceptor) blend used as the active region to determine the rotation speed and time in the spin coating technique were examined in the literature[28,54,55]. In order to determine the rotation speed and time to be used, the time of 60 s at 1500 rpm, which has the lowest interfacial defects and the highest efficiency, was determined. The substrates whose cleaning process was completed were coated by dropping 30 mL of the prepared PTB7:$PC_{71}BM$ blend to cover the whole substrate and coating by spin coating technique at 1500 rpm for 60 s. Instead of applying heat treatment for post-coating drying, the coated materials were left for ~ 12 h for slow drying. In order to prevent heat treatment from destroying the structure of the polymer, it is preferred that the drying process takes place in a clean room environment and at room temperature[54].

In this study, the deposition of transition metal oxide materials such as ZnO, $MoO_3$ and $WO_3$, which form the ETLs and HTLs of all the structures prepared within the scope of the study, Ag used as metal contact material and $MoO_3$/Ag/$MoO_3$ DMD transparent contacts was carried out by sputtering technique using the Nanovak NVTS-500 co-sputter system. The system also includes evaporation pots that allow thin film deposition using the evaporation technique. The system has 1 DC and 2 RF source targets with a diameter of 2 inches. The focus of the targets is a rotatable circular substrate holder that can be heated up to 600 °C. All deposition operations were performed in a vacuum of $10^{-8}$ Torr.

The optical characteristics of the fabricated structures were assessed using a Perkin Elmer Lambda 2 S UV-Vis-NIR spectrometer in the wavelength range of 300–1100 nm. Furthermore, J-V measurements were conducted using a Keithley 4200 source meter, while AM1.5G illumination was provided by a Newport Oriel-Sol1A solar simulator.

## Data availability

The materials and data supporting this study's findings are available from the corresponding authors upon request.

Received: 1 July 2024; Accepted: 14 October 2024
Published online: 27 October 2024

## References

1. Khandelwal, K., Biswas, S., Mishra, A. & Sharma, G. D. Semitransparent organic solar cells: from molecular design to structure–performance relationships. *J. Mater. Chem. C Mater.* **10**, 13–43 (2022).
2. Choy, W. C. H. *Organic Solar Cells Materials and Device Physics*. *Springer*Springer London, London, (2013).
3. Husain, A. A. F., Hasan, W. Z. W., Shafie, S., Hamidon, M. N. & Pandey, S. S. A review of transparent solar photovoltaic technologies. *Renew. Sustain. Energy Rev.* **94**, 779–791 (2018).
4. Sun, J. & Jasieniak, J. J. Semi-transparent solar cells. *J. Phys. D Appl. Phys.* **50**, 093001 (2017).
5. Srivishnu, K. S., Rajesh, M. N., Prasanthkumar, S. & Giribabu, L. Photovoltaics for indoor applications: Progress, challenges and perspectives. *Sol. Energy*. **264**, 112057 (2023).
6. Abubaker, S. A. & Pakhuruddin, M. Z. Progress and development of organic photovoltaic cells for indoor applications. *Renew. Sustain. Energy Rev.* **203**, 114738 (2024).
7. Biswas, S., Lee, Y., Choi, H., Lee, H. W. & Kim, H. Progress in organic photovoltaics for indoor application. *RSC Adv.* **13**, 32000–32022 (2023).
8. Çetinkaya, Ç. et al. Design and fabrication of a semi-transparent solar cell considering the effect of the layer thickness of $MoO_3$/Ag/$MoO_3$ transparent top contact on optical and electrical properties. *Sci. Rep.* **11**, 1–17 (2021).
9. Yu, W. et al. Effects of the optical microcavity on the performance of ITO-free polymer solar cells with $WO_3$/Ag/$WO_3$ transparent electrode. *Sol. Energy Mater. Sol. Cells*. **100**, 226–230 (2012).
10. Li, G., Zhu, R. & Yang, Y. Polymer solar cells. *Nat. Photonics*. **6**, 153–161 (2012).
11. García-Valverde, R., Cherni, J. A. & Urbina, A. Life cycle analysis of organic photovoltaic technologies. *Prog. Photovoltaics Res. Appl.* **18**, 535–558 (2010).
12. Cui, Y. et al. Efficient Semitransparent Organic Solar cells with tunable Color enabled by an Ultralow-Bandgap Nonfullerene Acceptor. *Adv. Mater.Bold"*>*29*, 1–7 (2017).
13. Çokduygulular, E., Çetinkaya, Ç., Emik, S. & Kınacı, B. In-depth analysis on PTB7 based semi-transparent solar cell employing $MoO_3$/Ag/$WO_3$ contact for advanced optical performance and light utilization. *Sci. Rep.* **13**, 7548 (2023).
14. Çetinkaya, Ç. et al. Enhancement of color and photovoltaic performance of semi-transparent organic solar cell via fine-tuned 1D photonic crystal. *Sci. Rep.* **12**, 1–13 (2022).
15. Çetinkaya, Ç., Çokduygulular, E., Güzelçimen, F. & Kınacı, B. Functional optical design of thickness-optimized transparent conductive dielectric-metal-dielectric plasmonic structure. *Sci. Rep.* **12**, 8822 (2022).
16. Çetinkaya, Ç. et al. Highly improved light harvesting and photovoltaic performance in CdTe solar cell with functional designed 1D-photonic crystal via light management engineering. *Sci. Rep.* **12**, 11245 (2022).
17. Çetinkaya, Ç. Efficient and high-bifacial CdTe-based solar cell enabled by functional designed dielectric/metal/dielectric transparent top contact via light management engineering. *Opt. Mater. (Amst)* **133**, 13003 (2022).
18. Upama, M. B. et al. High performance semitransparent organic solar cells with 5% PCE using non-patterned $MoO_3$/Ag/$MoO_3$ anode. *Curr. Appl. Phys.* **17**, 298–305 (2017).
19. Xu, G. et al. High-performance Colorful Semitransparent Polymer Solar cells with ultrathin hybrid-metal electrodes and fine-tuned dielectric mirrors. *Adv. Funct. Mater.* **27**, 1605908 (2017).
20. Betancur, R. et al. Transparent polymer solar cells employing a layered light-trapping architecture. *Nat. Photonics*. **7**, 995–1000 (2013).

21. Ramírez Quiroz, C. O. et al. Coloring Semitransparent Perovskite Solar cells via Dielectric Mirrors. *ACS Nano*. **10**, 5104–5112 (2016).
22. Duan, L., Hoex, B. & Uddin, A. Progress in Semitransparent Organic Solar cells. *Solar RRL*. **5**, 1–23 (2021).
23. Pettersson, L. A. A., Roman, L. S. & Inganäs, O. Modeling photocurrent action spectra of photovoltaic devices based on organic thin films. *J. Appl. Phys.* **86**, 487–496 (1999).
24. Liang, Y. & Yu, L. A new class of semiconducting polymers for bulk heterojunction solar cells with exceptionally high performance. *Acc. Chem. Res.Bold">43*, 1227–1236 (2010).
25. Liang, Y. et al. For the bright future-bulk heterojunction polymer solar cells with power conversion efficiency of 7.4%. *Adv. Mater.* **22**, 135–138 (2010).
26. Liu, Z., You, P., Liu, S. & Yan, F. Neutral-color Semitransparent Organic Solar cells with all-Graphene electrodes. *ACS Nano*. **9**, 12026–12034 (2015).
27. Fan, X. et al. Highly Conductive Stretchable All-Plastic electrodes using a Novel dipping-embedded transfer method for high-performance Wearable sensors and Semitransparent Organic Solar cells. *Adv. Electron. Mater.* **3**, 1–7 (2017).
28. Zheng, J. W. et al. Toward ultra-low reflectance semi-transparent organic photovoltaic cells with biomimetic nanostructured transparent electrode. *Org. Electron.* **60**, 38–44 (2018).
29. Upama, M. B. et al. High-efficiency Semitransparent Organic Solar cells with non-fullerene acceptor for window application. *ACS Photonics*. **4**, 2327–2334 (2017).
30. You, H. et al. Low temperature aqueous solution-processed ZnO and polyethylenimine ethoxylated cathode buffer bilayer for high performance flexible inverted organic solar cells. *Energies (Basel)*. **10**, 1–12 (2017).
31. Tai, Q. & Yan, F. Emerging Semitransparent Solar cells: materials and device design. *Adv. Mater.* **29**, 1–37 (2017).
32. Çetinkaya, Ç. et al. Evaluation on output parameters of the inverted organic solar cells depending on transition-metal-oxide based hole-transporting materials. *Opt. Mater. (Amst)*. **120**, 111457 (2021).
33. White, M. S., Olson, D. C., Shaheen, S. E., Kopidakis, N. & Ginley, D. S. Inverted bulk-heterojunction organic photovoltaic device using a solution-derived ZnO underlayer. *Appl. Phys. Lett.* **89**, 143517 (2006).
34. Shi, L. et al. High performance ultrathin $MoO_3$/Ag transparent electrode and its application in semitransparent organic solar cells. *Nanomaterials* **8**(7), 473 (2018).
35. Jain, N. et al. Interfacial disorder in efficient polymer solar cells: the impact of donor molecular structure and solvent additives. *J. Mater. Chem. Mater.* **5**, 24749–24757 (2017).
36. Xiao, L. et al. Light managements and transparent electrodes for Semitransparent Organic and Perovskite Solar cells. *Solar RRL*. **6**, 1–24 (2022).
37. Xia, R., Brabec, C. J., Yip, H. L. & Cao, Y. High-throughput optical screening for efficient Semitransparent Organic Solar cells. *Joule*. **3**, 2241–2254 (2019).
38. Hu, Z. et al. A critical review on semitransparent organic solar cells. *Nano Energy*. **78**, 105376 (2020).
39. Alahmadi, A. N. M. Design of an efficient PTB7:$PC_{70}$BM-Based polymer solar cell for 8% efficiency. *Polym. (Basel)* **14**(5), 889 (2022).
40. Tao, C. et al. Performance improvement of inverted polymer solar cells with different top electrodes by introducing a $MoO_3$ buffer layer. *Appl. Phys. Lett.* **93**, 2006–2009 (2008).
41. Dong, W. et al. Bifunctional $MoO_3$ –$WO_3$/Ag/$MoO_3$–WO3 films for efficient ITO–Free Electrochromic devices. *ACS Appl. Mater. Interfaces*. **8**, 33842–33847 (2016).
42. Choi, D. K. et al. Highly efficient, heat dissipating, stretchable organic light-emitting diodes based on a MoO3/Au/MoO3 electrode with encapsulation. *Nat. Commun.* **12**, 2864 (2021).
43. Najafi-Ashtiani, H., Akhavan, B., Jing, F. & Bilek, M. M. Transparent conductive dielectric – metal – dielectric structures for Electrochromic Applications fabricated by high-power impulse Magnetron Sputtering. *ACS Appl. Mater. Interfaces*. **11**, 14871–14881 (2019).
44. Yeh, T. H. et al. Vacuum-deposited $MoO_3$/Ag/$WO_3$ multilayered electrode for highly efficient transparent and inverted organic light-emitting diodes. *Org. Electron.* **59**, 266–271 (2018).
45. Guo, S., Cao, B., Wang, W., Moulin, J. F. & Müller-Buschbaum, P. Effect of alcohol treatment on the performance of PTB7:$PC_{71}$BM bulk heterojunction solar cells. *ACS Appl. Mater. Interfaces*. **7**, 4641–4649 (2015).
46. Guo, S. et al. Solvent-morphology-property relationship of PTB7:$PC_{71}$BM polymer solar cells. *ACS Appl. Mater. Interfaces*. **9**, 3740–3748 (2017).
47. Kwon, Y., Seo, J., Kang, Y., Kim, D. & Kim, J. Bifacial CdS/CdTe thin-film solar cells using a transparent silver nanowire/indium tin oxide back contact. *Opt. Express*. **26**, A30 (2018).
48. Fujii, S. & Hara, Y. Air-processed semitransparent organic solar cells with tunable color. *Mater. Express*. **8**, 189–194 (2018).
49. Vimala, M., Ramadas, G., Perarasi, M., Manokar, A. M. & Sathyamurthy, R. A. Review of different types of solar cell materials employed in Bifacial Solar Photovoltaic Panel. *Energies (Basel)* **16**(8), 3605 (2023).
50. Böscke, T. S. et al. Bifacial n-Type cells with > 20% front-side efficiency for Industrial Production. *IEEE J. Photovolt.* **3**, 674–677 (2013).
51. Subedi, K. K. et al. Enabling bifacial thin film devices by developing a back surface field using CuxAlOy. *Nano Energy*. **83**, 105827 (2021).
52. Nishimura, T. et al. Device design for high-performance bifacial cu(in,Ga)Se2 solar cells under front and rear illuminations. *Sol. Energy*. **218**, 76–84 (2021).
53. Ho, C. H. Y. et al. Impact of Solvent Additive on Carrier Transport in Polymer:Fullerene Bulk Heterojunction Photovoltaic cells. *Adv. Mater. Interfaces*. **2**, 1–8 (2015).
54. Lin, S. et al. Solution-processable ultrathin black phosphorus as an Effective Electron Transport Layer in Organic Photovoltaics. *Adv. Funct. Mater.* **26**, 864–871 (2016).
55. To, C. H. et al. Effect of PTB7 Properties on the performance of PTB7:$PC_{71}$BM solar cells. *ACS Appl. Mater. Interfaces*. **7**, 13198–13207 (2015).


## Acknowledgements

This work was supported by The Scientific and Technological Research Council of Türkiye (TÜBITAK) 2211/C National PhD Scholarship Program in the Priority Fields in Science and Technology, and Istanbul University-Cerrahpaşa Scientific Research Project Coordination Unit (Project No: FDK-2023-37353).

## Author contributions

E.Ç. conducted the study, designed the semi-transparent solar cell structures by making calculations, performed experimental studies, and wrote the main article text, Ç.Ç. designed the semi-transparent solar cells and performed experimental studies, analysed the calculation results and wrote the main article text, S.E. made the critical revision and supervised the study, B.K. edited the main article text and supervised the study.

## Declarations

### Competing interests
The authors declare no competing interests.

### Additional information
**Correspondence** and requests for materials should be addressed to E.Ç.

**Reprints and permissions information** is available at www.nature.com/reprints.

**Publisher's note** Springer Nature remains neutral with regard to jurisdictional claims in published maps and institutional affiliations.

**Open Access** This article is licensed under a Creative Commons Attribution-NonCommercial-NoDerivatives 4.0 International License, which permits any non-commercial use, sharing, distribution and reproduction in any medium or format, as long as you give appropriate credit to the original author(s) and the source, provide a link to the Creative Commons licence, and indicate if you modified the licensed material. You do not have permission under this licence to share adapted material derived from this article or parts of it. The images or other third party material in this article are included in the article's Creative Commons licence, unless indicated otherwise in a credit line to the material. If material is not included in the article's Creative Commons licence and your intended use is not permitted by statutory regulation or exceeds the permitted use, you will need to obtain permission directly from the copyright holder. To view a copy of this licence, visit http://creativecommons.org/licenses/by-nc-nd/4.0/.

© The Author(s) 2024